DOI: 10.1002/chem.200600044

Oxidative DNA Cleavage Promoted by Multinuclear Copper Complexes: Activity Dependence on the Complex Structure

Yongmei Zhao,[a] Jianhui Zhu,[a] Weijiang He,*[a] Zhen Yang,[a] Yangguang Zhu,[a] Yizhi Li,[a] Junfeng Zhang,[b] and Zijian Guo*[a]

Abstract: Polynuclear copper complexes with two or three Cu(BPA) (BPA, bis(2-pyridylmethyl)amine) motifs, $[Cu_2(m\text{TPXA})Cl_4]\cdot 3H_2O$ (**1**), $[Cu_2(p\text{TPXA})Cl_4]\cdot 3H_2O$ (**2**), $[Cu_3(\text{HPTAB})Cl_5]Cl\cdot 3H_2O$ (**3**) (*m*TPXA = *N*,*N*,*N*′,*N*′-tetra-(2-pyridylmethyl)-*m*-xylylene diamine; *p*TPXA = *N*,*N*,*N*′,*N*′-tetra-(2-pyridylmethyl)-*p*-xylylenediamine; HPTAB = *N*,*N*,*N*′,*N*′,*N*″,*N*″-hexakis(2-pyridylmethyl)-1,3,5-tris-(aminomethyl)benzene) have been synthesized and characterized. The crystal structures of compounds **2** and **3** showed each Cu(BPA) motif had a 4+1 square-pyramidal coordination environment with one chloride occupying the apical position and three N atoms from the same BPA moiety together with another Cl atom forming the basal plane. Fluorescence and circular dichroism (CD) spectroscopy studies indicated that the DNA binding followed an order of **3** > **2** > **1** in the compounds. These complexes cleave plasmid pUC19 DNA by using an oxidative mechanism with mercaptopropionic acid (MPA) as the reductant under aerobic conditions. Dinuclear Cu^{2+} complexes **1** and **2** showed much higher cleavage efficiency than their mononuclear analogue $[Cu(bpa)Cl_2]$ at the same $[Cu^{2+}]$ concentration, suggesting a synergistic effect of the Cu^{2+} centers. Moreover, the *meta*-dicopper centers in complex **1** facilitated the formation of linear DNA. Interestingly, the additional copper center to the *meta*-dicopper motif in complex **3** decreased the cleavage efficacy of *meta*-dicopper motif in complex **1**, although it is able to cleave DNA to the linear form at higher $[Cu^{2+}]$ concentrations. Therefore, the higher DNA binding ability of complex **3** did not lead to higher cleavage efficiency. These findings have been correlated to the DNA binding mode and the ability of the Cu^{2+} complexes to activate oxygen (O_2). This work is a good example of the rational design of multinuclear Cu^{2+} artificial nuclease and the activity of which can be manipulated by the geometry and the number of metal centers.

Keywords: artificial nucleases · copper · DNA cleavage · polynuclear complexes · synergetic effects

Introduction

Artificial nucleases have received considerable current interest for their diverse applications not only as therapeutic agents but also in genomic research.[1–3] Among them, transition metal complexes have been studied extensively due to their diversity in structure and reactivity.[2] The biologically accessible oxidative/reductive potential made copper complexes a class of the most frequently studied metallonucleases. The $[Cu(OP)_2]^{2+}$ (OP = 1,10-phenanthroline) was the first Cu^{2+} complex displaying high efficiency for oxidative cleavage of DNA.[4,5] Other copper complexes, such as copper–ATCUN (*a*mino-*t*erminal Cu^{II}- and Ni^{II}-binding) peptide complexes and Cu–PPA (polypyridyl-derived amine), that were developed as copper enzyme mimics, were also found to cleave DNA efficiently.[6,7] These complexes displayed versatile cleavage properties due to their different structure and reaction conditions.

Multinuclear complexes have attracted attention as artificial nuclease since multinuclear metal centers are often found in natural nucleases and the metal centers may demonstrate synergistic effects in O_2 activation and DNA recognition.[2,6,8] In the copper complexes of PPA, the intramolecular copper centers displayed synergistic effects in DNA

[a] Y. Zhao, J. Zhu, Dr. W. He, Z. Yang, Y. Zhu, Dr. Y. Li, Prof. Dr. Z. Guo
State Key Laboratory of Coordination Chemistry
School of Chemistry and Chemical Engineering
Nanjing University, Nanjing 210093 (P.R. China)
Fax: (+86) 025-8331-4502
E-mail: heweij69@nju.edu.cn
zguo@nju.edu.cn

[b] Prof. Dr. J. Zhang
State Key Laboratory of Pharmaceutical Biotechnology Nanjing University, Nanjing 210093 (P.R. China)

Supporting information for this article is available on the WWW under http://www.chemeurj.org/ or from the author.

cleavage with higher efficiency or selectivity.[6c,e,9–15] For example, both $[Cu_2(D^1)(H_2O)_2](ClO_4)_4$ and $[Cu_2(DO)(Cl_2)](ClO_4)_2$ showed synergy between copper centers with higher efficiency in DNA cleavage (see below). The former one

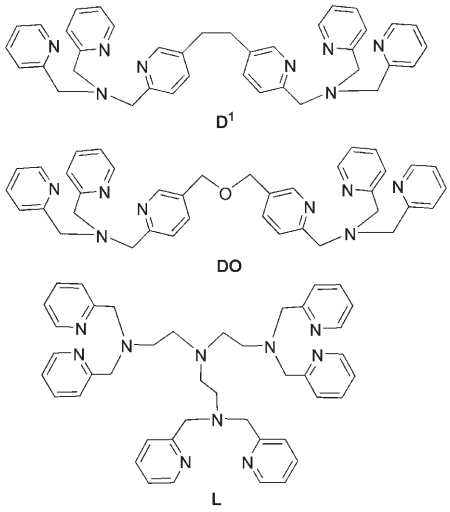

and $[Cu_3(L)(H_2O)_3(NO_3)_2](NO_3)_4{\cdot}5H_2O$ also displayed selective cleavage at the junction between single- and double-stranded DNA.[6] The different cleavage behaviors implied that the linker between the copper centers in polycopper complexes played an essential role in determining their different synergetic effects in cleavage. The flexible linkers between coordinating moieties in D^1, DO, and L polydentate ligands made the three complex structures variable especially in solution. Therefore, it is difficult to explain the structural dependence of the synergistic effect on DNA cleavage. Ligands with a rigid linker may restrict the intramolecular Cu···Cu distances and fix the geometry. For this reason, in our previous work, the rigid mesitylene group was adopted to link three Cu(DPA) (DPA = dipyridylamine) motifs and the resulting complex showed remarkable DNA cleavage efficiency.[16] However, the factors that govern the synergy between multinuclear copper centers are unknown, and the low solubility of the complex in water precludes further investigation of the system.

In this work, two binuclear and one trinuclear copper complex $[Cu_2(m\text{TPXA})Cl_4]{\cdot}3H_2O$ (**1**), $[Cu_2(p\text{TPXA})Cl_4]{\cdot}3H_2O$ (**2**), and $[Cu_3(\text{HPTAB})Cl_5]Cl{\cdot}3H_2O$ (**3**) (*m*TPXA = *N*,*N*,*N*′,*N*′-tetra-(2-pyridylmethyl)-*m*-xylylene diamine; *p*TPXA = *N*,*N*,*N*′,*N*′-tetra-(2-pyridylmethyl)-*p*-xylylenediamine; HPTAB = *N*,*N*,*N*′,*N*′,*N*″,*N*″-hexakis(2-pyridylmethyl)-1,3,5-tris-(aminomethyl)benzene)) have been designed and synthesized, in which the Cu(BPA) (BPA = bis(2-pyridylmethyl)amine) motif was adopted to improve the water solubility of the resulting complexes. In order to elucidate the structural dependence of synergy between metal centers in DNA cleavage, the Cu(BPA) motifs in the complexes were elaborately linked by rigid *meta*-, *para*-xylylene, and mesitylene groups (see below). In the dicopper complexes **1** and **2**, the intramolecular copper centers were linked by *meta*- and *para*-xylene groups, respectively. With the mesitylene spacer, every two intramolecular copper centers in complex **3** form the *meta*-dicopper motif similar to that in complex **1**. The cleavage activity of mononuclear complex **4** was also examined for comparison.

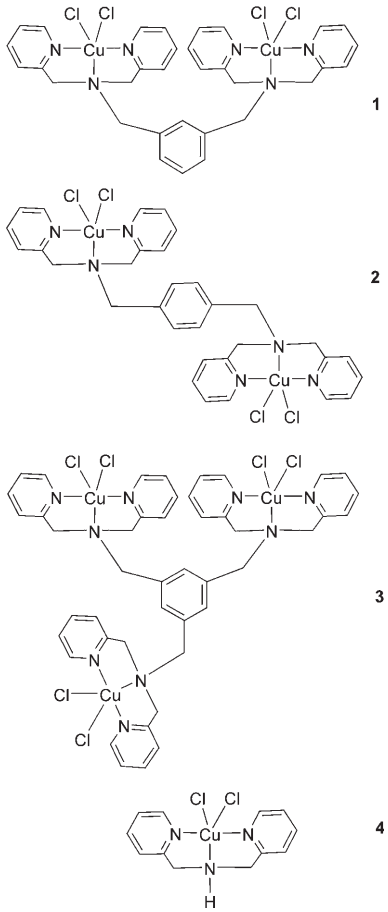

Results and Discussion

General aspects: Dinuclear complexes **1** and **2**, are quite soluble and stable in water, and their electrospray mass spectra displayed two signals at *m*/*z* 349.2 and 732.9 that can be assigned to $[M-2Cl]^{2+}$ and $[M-Cl]^{+}$ (M = $Cu_2(\text{TPXA})Cl_4$), respectively. Their isotopic distribution patterns are almost identical to the corresponding simulated ones given by Isopro 3.0 (Figure S1 in the Supporting Information). The trinuclear copper complex **3** that has been characterized as a coordination polymer by X-ray crystallography (see below) was also soluble in water. The ES-MS spectrum in positive mode gave three signals at *m*/*z* 336.3, 521.9, and 1078.8, that could be assigned to $[M-3Cl]^{3+}$, $[M-2Cl]^{2+}$, $[M-Cl]^{+}$ (M = $Cu_3(\text{HPTAB})Cl_6$) based on the molecular mass and isotopic distribution patterns. These values are very similar to the simulated ones given by

Isopro 3.0 (Figure S1 in the Supporting Information). Therefore, the complex may exist as a monomer in water.

Structure of complexes 2 and 3: Complexes **2** and **3** have been structurally characterized by X-ray crystallography. The data collection and refinement parameters are given in Table 1. For complex **2**, there is one neutral dinuclear Cu^{II} complex and three H_2O molecules in the crystallographic symmetric unit (Figure 1a). Selected bond lengths and angles are given in Table 2. The Cu···Cu distance is 7.98 Å and each copper atom has a five-coordinated geometry that can be described as distorted square-pyramidal according to the Addison–Reedijk geometric criterion.[17] The copper center and N1,N2,N3,Cl2 atoms form the basal plane. The apical position is occupied by Cl1 with a Cu–Cl1 distance of 2.52 Å. The basal plane shows a tetrahedral distortion with the copper center deviating from the basal plane by 0.22 Å and the axial bond Cu–Cl1 is nearly perpendicular to the basal plane.

Table 1. Data collection and refinement parameters for complexes **2** and **3**.

	Complex **2**	Complex **3**
empirical formula	$C_{32}H_{38}Cl_4Cu_2N_6O_3$	$C_{45}H_{51}Cl_6Cu_3N_9O_3$
formula weight	823.56	1169.4
T [K]	293(2)	293(2)
crystal system	monoclinic	monoclinic
space group	C_2/c	$P2(1)/c$
a [Å]	26.817(7)	19.117 (2)
b [Å]	10.825(3)	16.191 (2)
c [Å]	15.761(4)	17.741 (2)
β [°]	122.717(5)	105.86 (1)
V [Å^3]	3849.6(17)	5282.1(9)
Z	4	4
ρ_{calcd} [g cm^{-3}]	1.421	1.470
$F(000)$	1688	2388
goodness-of-fit on F^2	1.074	1.046
final R indices [$I>2\sigma(I)$]		
R_1	0.0530	0.0429
wR_2	0.1152	0.0898
R indices (all data)[a]		
R_1	0.0826	0.0611
wR_2	0.1238	0.0948

[a] $R_1=\Sigma||F_o|-|F_c||/\Sigma|F_o|$; $wR_2=[w(F_o^2-F^2)^2]/\Sigma w(F_o^2)^2]^{1/2}$.

Table 2. Selected bond lengths [Å] and angles [°] for complex **2**.

Cu1–Cl1	2.5151	Cu1–Cl2	2.253(2)
Cu1–N1	2.021(3)	Cu1–N2	2.078(3)
Cu1–N3	2.006(3)		
Cl1-Cu1-Cl2	105.04(5)	Cl1-Cu1-N1	95.32(9)
Cl1-Cu1-N2	97.61(9)	Cl1-Cu1-N3	91.01(10)
Cl2-Cu1-N1	97.30(10)	Cl2-Cu1-N2	157.35(9)
Cl2-Cu1-N3	97.66(11)	N1-Cu1-N2	80.61(12)
N1-Cu1-N3	161.64(13)	N2-Cu1-N3	81.47(13)

The crystal structure as determined by X-ray diffraction analysis of complex **3** is presented in Figure 1b. Each BPA motif binds one Cu^{II} ion and the intrametal distance is 7.353 Å (Cu1···Cu2), 6.883 Å (Cu1 ···Cu3), and 8.041 Å (Cu2···Cu3), respectively. The three copper ions are all coordinated in a square-pyramidal geometry with one Cl atom at each apical point. The Cu1 and Cu2 centers are on the same side of the benzene plane while Cu3 is on the other side. The Cl4 acts as the bridging atom coordinating with the Cu1 and Cu2 centers of another trinuclear unit to form a one-dimensional helical chain along the b axis (Figure S2 in the Supporting Information). Selected bond lengths and angles are also listed in Table 3. As can be noted, the Cu2–Cl4b distance of 2.742 Å is much longer than other Cu–Cl distances (2.232–2.586 Å) observed in the molecule. Hence, in spite of the one-dimensional polymeric nature of complex **3** in the solid structure, the intermolecular bond, Cu2–Cl4b, is very weak and can be broken easily in aqueous solution as observed in the ES-MS data (see above).

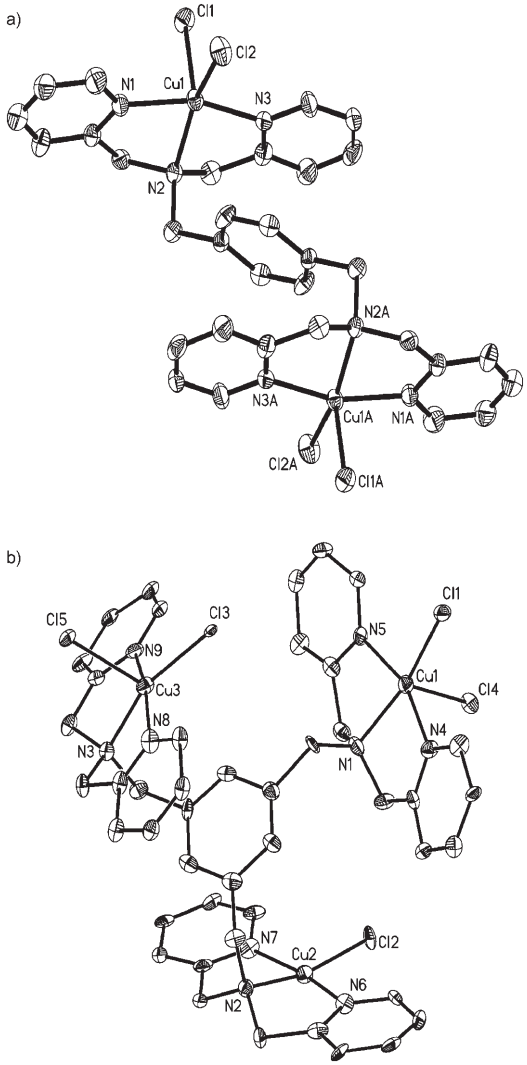

Figure 1. Structures of complexes **2** (a) and **3** (b) as determined by X-ray crystallography. Thermal ellipsoids are drawn at the 30% probability level. Atom numbering of carbon atoms, solvent molecules, and hydrogen atoms are omitted for clarity.

Table 3. Selected bond lengths [Å] and angles [°] for complex **3**.

Cu1−Cl1	2.239(3)	Cu1−Cl4	2.586(9)
Cu1−N1	2.032(3)	Cu1−N4	2.019(3)
Cu1−N5	1.995(3)	Cu2−Cl2	2.238(2)
Cu2−Cl4b	2.742(4)	Cu2−N2	2.052(3)
Cu2−N6	1.981(3)	Cu2−N7	1.952(3)
Cu3−Cl3	2.232(1)	Cu3−Cl5	2.562(9)
Cu3−N3	2.040(3)	Cu3−N8	2.002(3)
Cu3−N9	2.039(3)	Cl1-Cu1-N1	162.83(8)
N4-Cu1-N5	160.32(10)	Cl4-Cu1-N1	94.58(8)
Cl4-Cu1-N4	95.75(8)	Cl2-Cu2-N2	165.33(7)
N6-Cu2-N7	164.45(11)	Cl3-Cu3-N3	158.40(8)
N8-Cu3-N9	163.08(11)	Cl5-Cu3-N3	96.22(8)
Cl5-Cu3-N8	91.24(8)		

Electrochemistry: The electrochemical behavior of the complexes has been studied (Figure S3 in the Supporting Information). For complexes **1** and **2** at a scan rate of 100 mV s^{-1}, one broad cathodic peak and two anodic peaks were observed in the cyclic voltammograms (CV) in a 0.1 M aqueous KCl solution. The reductive potentials for the $Cu^{II}/Cu^{II}//Cu^{II}/Cu^{I}$ and $Cu^{II}/Cu^{I}//Cu^{I}/Cu^{I}$ processes in complexes **1** and **2** were very close so that only one broad cathodic peak was observed. Furthermore, the two electron-transfer processes involved were indicated by the two prominent anodic peaks upon scan reversal in both cases. Owing to the similarities of the cathodic peak potentials of complexes **1** and **2**, these two complexes can be reduced under similar conditions. Moreover, the more negative anodic peak potentials of $Cu^{II}/Cu^{II}//Cu^{II}/Cu^{I}$ and $Cu^{II}/Cu^{I}//Cu^{I}/Cu^{I}$ of complex **1** (−194 and 82 mV) suggested that the reduced copper(I) species of complex **1** could be oxidized more easily than that of complex **2** (−138 and 178 mV). Under the same conditions, the CV of complex **3** contained one broad cathodic peak and multiple anodic peaks at a scan rate of 100 mV s^{-1} (Figure S4 in the Supporting Information). Only one broad cathode peak was observed that may be the result of several close cathodic peaks, and the anodic peaks were also formed by several partly overlapped anode peaks in the reverse scan. Linear scan voltammetry (LSV) toward positive potentials following 10 s of pre-reduction at −800 mV displayed clearly three anode peaks (−175, −20, and 200 mV) for complex **3** indicating three electron-transfer processes corresponding to $Cu^{II}/Cu^{II}/Cu^{II}//Cu^{II}/Cu^{II}/Cu^{I}$, $Cu^{II}/Cu^{II}/Cu^{I}//Cu^{II}/Cu^{I}/Cu^{I}$ and $Cu^{II}/Cu^{I}/Cu^{I}//Cu^{I}/Cu^{I}/Cu^{I}$, respectively (Figure S4 in the Supporting Information).

CT DNA binding ability of complexes 1, 2, and 3: DNA binding is the critical step for DNA cleavage in most cases. Since these complexes have very similar UV absorbances to calf thymus (CT) DNA at 260 nm, the DNA binding studies were mainly carried out by using fluorescence and CD spectroscopy.

Firstly, the binding of the complexes to CT DNA was studied by evaluating the fluorescence emission intensity of the ethidium bromide (EB)–DNA system upon the addition of the complexes. If the complexes added to the EB–DNA system replace the bound EB, the emission intensity will be reduced. The fluorescence quenching of EB bound to DNA by the Cu^{II} complexes are shown in Figure 2, in which the fluorescence intensity at 600 nm (excited at 526 nm) of EB

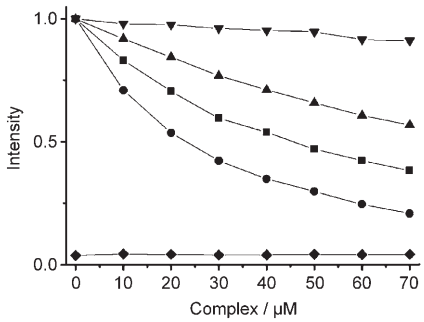

Figure 2. Emission profiles of 50 μM CT-DNA-bound EB in a 5 mM Tris-HCl buffer (pH 7.4) upon the addition of complexes **1** (▲), **2** (■), **3** (●), and **4** (▼) at 25 °C (◆, the emission intensity of EB without CT DNA in the presence of different concentrations of **2**).

in the bound form was plotted against the complex concentration. The evident fluorescence-quenching effect caused by the titration with complexes **1**, **2**, and **3** indicated their DNA-binding process by replacing the bound EB molecules. The apparent binding constants (K_{app}) can be calculated from the current data by using the reported method.[18] The values obtained for complexes **2** and **3** are 1.1×10^7 and 2.2×10^7 M^{-1}, respectively, while the value for complex **1** is less than 0.7×10^7 M^{-1}. The results demonstrated that complex **3** had a stronger affinity to DNA than complexes **1** and **2**. Moreover, complex **2** possesses higher DNA binding ability than complex **1**. The slight decrease in fluorescence caused by complex **4** indicated its lowest DNA binding affinity.

Figure 3 displays the CD spectra of CT DNA treated with complexes **1**, **2**, and **3** with the ratio of 0.4 (complex/DNA). Both the positive (~275 nm) and negative (~245 nm) bands decreased in intensity with the increase of the complex concentration. This suggests Cu complexes can unwind the DNA helix and lead to the loss of helicity.[19] The largest decrease in the CD band intensity caused by complex **3** at the same concentration implied that complex **3** was more effective than complexes **1** and **2** in perturbing the secondary structure of DNA. From the results of fluorescence and CD spectroscopic studies one can conclude that complex **3** binds to CT DNA more effectively than complex **2**, and complex **1** has the lowest affinity to DNA.

Nuclease activity of complexes 1, 2, and 3

*Cleavage of plasmid pUC19 DNA by copper complexes **1**, **2**, and **3***: The DNA cleavage activity of complexes **1**–**3** has been studied under physiological pH and temperature by gel electrophoresis by using supercoiled pUC19 plasmid DNA as the substrate. The cleavage activity of mononuclear complex **4** has also been examined for comparison. Figure 4 shows the results obtained at pH 7.4 (50 mM Tris-HCl,

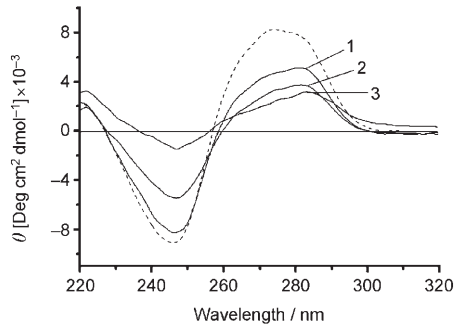

Figure 3. CD spectra of CT DNA (1.0×10^{-4} M) in the absence (·····) and presence (——) of complexes **1**, **2**, and **3** at ratio [Cu complex]/[DNA] = 0.4.

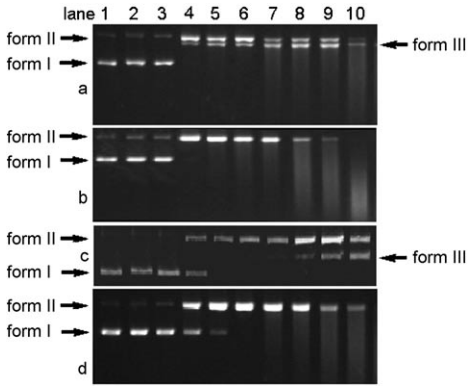

Figure 4. Agarose gel electrophoresis patterns for the cleavage of pUC19 plasmid DNA (0.02 mg mL^{-1}, 30 μM base pair) by complexes **1**, **2**, **3**, and **4** in the presence of 100-fold excess of MPA in the dark for 30 min in Tris-HCl buffer (50 mM, pH 7.4) at 37 °C: a) Lane 1, DNA control; lane 2, DNA + **1**(13 μM); lane 3, DNA + MPA; lanes 4–10, DNA + MPA + (1, 3, 5, 6, 8, 10, and 11 μM) of complex **1**; b) lane 1, DNA control; lane 2, DNA + **2**(10 μM); lane 3, DNA + MPA; lanes 4–10, DNA + MPA + (0.5, 1, 3, 5, 6, 8, and 10 μM) of complex **2**; c) lane 1, DNA control; lane 2, DNA + MPA(1 mM); lane 3, DNA + **3**(10 μM); lanes 4–10, DNA + (1, 2, 3, 4, 5, 8, and 10 μM) of complex **3**; d) lane 1, DNA control; lane 2, DNA + **4**(24 μM); lane 3, DNA + MPA; lanes 4–10, DNA + MPA + (1, 2, 4, 6, 10, 12, and 16 μM) of complex **4**.

50 mM NaCl) at 37 °C for 30 min. The complex or MPA alone (Figure 4a–d, lanes 1–3) does not show any cleavage activity. In the presence of MPA, all complexes can cleave supercoiled DNA (form I) to nicked (form II) or linear DNA (form III). These data suggested the cleavage mediated by these complexes should be oxidative. Complex **1** completely converted form I DNA to form II at 0.5 μM concentration (Figure S5 in the Supporting Information) and further to the linear DNA at 1 μM (Figure 4a, lane 4). At higher concentration of complex **1** ($\leq$10 μM), the presence of form III increased with concomitant decrease of the nicked form (Figure 4a, lanes 4–9). Form II DNA disappeared at a concentration of 11 μM of complex **1** and form III was also degraded into fragments to form smear in the gel. The DNA was completely turned into small fragments as absolute smear at a concentration of 13 μM of complex **1** (data not shown).

For complex **2**, the supercoiled DNA was completely degraded into the nicked form at 0.5 μM (Figure 4b, lane 4). The co-existing smears became evident with the increase of the concentration of complex **2**, yet form II was still observable until the concentration of complex **2** reached 6 μM (Figure 4b, lanes 5–8). At a higher concentration of complex **2** ($\geq$8 μM), the nicked DNA degraded completely into small pieces and only smear was found (Figure 4b, lanes 9–10). In contrast to the reactivity of complex **1**, complex **2** could not induce the conversion of form I to form III at the tested concentrations (Figure 4b). Complex **3** could mediate the conversion of most of the supercoiled DNA to the nicked form at 3 μM (Figure 4c, lane 6). At higher concentrations, complex **3** resulted in the complete conversion of form I to forms II and III (Figure 4c, lane 7). The concentration increase of complex **3** led to an increase of form III (Figure 4c, lanes 8–10) and the concomitant decrease of form II in the range of 4–10 μM. At concentrations higher than 10 μM, complex **3** gradually degraded form II and form III DNA into small pieces of different sizes (Figure S6 in the Supporting Information). The quantified data for different forms of DNA produced are listed in Tables 4 and 5.

Table 4. Cleavage of pUC19 plasmid DNA by complexes **1** and **3** at different concentrations in the presence of 100-fold excess of MPA.

Complex	Concentration [μM]	Supercoiled [%]	Nicked [%]	Linear [%]
none	0	91	9	0
1	1	0	82	18
1	3	0	66	34
1	5	0	53	47
1	6	0	42	57
1	8	0	45	55
1	10	0	45	55
3	1	56	44	0
3	2	25	75	0
3	3	11	89	0
3	4	0	82	18
3	5	0	75	25
3	8	0	69	31
3	10	0	57	43

Table 5. Time-dependent cleavage of pUC19 plasmid DNA by 8 μM of complex **3** in the presence of 100-fold excess of MPA.

Reaction time [min]	Supercoiled [%]	Nicked [%]	Linear [%]
DNA (alone)	100	0	0
3	12	78	10
5	7	79	14
8	0	82	18
10	0	81	19
15	0	79	21
20	0	76	24
25	0	72	28
30	0	68	32

Similar to complex **2**, complex **4** could not degrade the supercoiled DNA to its linear form (Figure 4d) at any concentration tested, although 4 μM of complex **4** could mediate complete conversion of form I to form II (Figure 4d, lane 6).

The coexisting smear was found at even higher concentrations, yet form II remained up to a concentration of 16 μM (Figure 4d, lanes 7–12).

Synergistic effect in DNA cleavage efficiency: The comparison of cleavage activity of complexes **1**, **2**, and **4** at equivalent copper ion concentrations revealed that complexes **1** and **2** are more active than their mononuclear analogue complex **4**. The time-dependent experiments on DNA cleavage by 1 μM [Cu^{2+}] of complexes **1** and **2** over the course of 30 min in the presence of 100-fold excess of MPA (Figure S5 in the Supporting Information) demonstrated that form I almost completely converted into form II in 5 min for the two compounds, whereas the equivalent [Cu^{2+}] of complex **4** only converted approximately 50% of the form I into form II. Total conversion to nicked DNA could be reached at 4 μM [Cu^{2+}] in 30 min for complex **4**. This result implies a quite efficient DNA cleavage process mediated by complexes **1** and **2**, suggesting a possible synergy between the two copper centers in complexes **1** and **2** concerning the DNA nicking.[6d]

Besides the similar *meta*-dicopper centers in complex **1**, complex **3** possesses an additional copper center and all three copper centers are connected to 1,3,5-positions of the benzene ring to form a head-to-tail *meta*-tricopper structure. To our surprise, the additional copper greatly quenched the cleavage efficiency of complex **3** compared with the dicopper complexes **1** or **2**. The nicking efficiency of complex **3** was only comparable to that of complex **4**.

Plasmid pUC19 DNA cleavage in the presence of standard radical scavengers and reaction inhibitors: Experiments with different scavenging agents were also carried out to identify the intermediate reactive oxygen species (ROS) that might be formed in the DNA cleavage reaction (Figure 5). The addition of NaN_3 or KI to the system was found to have little effect on DNA cleavage, suggesting that singlet oxygen and H_2O_2 are not the effective ROS for the cleavage. The addition of 1.0 M DMSO has no evident inhibition effect on the cleavage but 1.5 M DMSO could only partially inhibit the cleavage process mediated by complexes **1**–**3**. This ruled out the possible involvement of diffusible hydroxyl radicals, and the DNA-bound reactive oxygen species (ROS) should be responsible for the cleavage reaction as proposed for [Cu(*ortho*-phenanthroline)$_2$]$^{2+}$.[20]

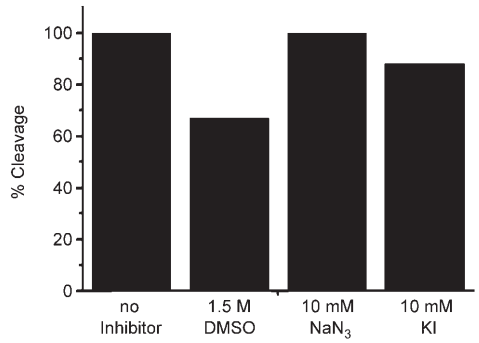

Figure 5. Histogram representing overall strand scission (nicked form) of pUC19 plasmid DNA by 3 μM of complex **3** and 100-fold excess of MPA in the presence of standard radical scavengers.

DNA binding and DNA cleavage efficiency: It was proposed that the DNA binding ability of copper complexes was essential to mediate DNA cleavage when DNA-bound ROS acted as the direct oxidative intermediates, and higher DNA affinity normally leads to higher DNA cleavage efficiency.[7] Since polynuclear complexes can enhance the affinity to anionic DNA, they may enhance the DNA cleavage efficiency. In our case, the DNA binding affinity of the complexes indeed showed the following order, **3** > **2** > **1** > **4**. Although dicopper complexes **1** and **2** have a higher DNA cleavage efficiency than complex **4**, *meta*-tricopper complex **3** displayed the lowest cleavage efficiency in the three multinuclear copper complexes. Therefore, the DNA binding affinity of the copper complexes does not necessarily correlate to their cleavage efficacy.

The formation process of DNA-bound ROS and the subsequent proton abstraction from deoxyribose by ROS should play important roles in determining the cleavage efficiency and the cleavage kinetics.[2] The former one is not only related to the formation of DNA-copper adduct but also related to the activation of O_2 by this DNA-bound copper adduct (Figure 6). Studies on polycopper complexes

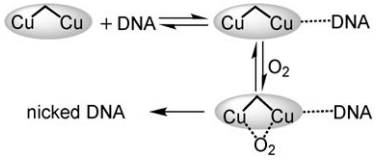

Figure 6. Proposed mechanism to form DNA-bound ROS for DNA cleavage.

have demonstrated that the ability of intramolecular copper centers to activate molecular oxygen could be enhanced by the synergy between the suitably linked copper centers.[21–23] For example, it was reported that the *para*-dicopper and the *meta*-dicopper motif, especially the latter, had a strong ability to bind O_2 and to form ROS species due to the synergistic effect caused by the suitable distance between the two copper centers. This could also be the origin for the higher DNA cleavage efficiency caused by complexes **1** and **2**. However, the contribution of the higher DNA affinity of complexes **1** and **2** could not be ruled out.

Complex **3** contains not only the *meta*-dicopper motif as that in complex **1** that may favor the O_2 activation process, but also the third copper center that enhanced the DNA binding affinity. The formation of DNA-bound Cu^{2+}-centered ROS should be enhanced. However, its nicking efficacy was unexpectedly quenched and was lower than that for complex **1**. This observation suggests that the third copper center in complex **3** may alter the orientation of the *meta*-di-

copper motif that inhibits access of the ROS to the target proton of deoxyribose and hence lowers the cleavage efficiency. Therefore, the proton abstraction process by the ROS that was essentially affected by the DNA binding mode and the binding sites[2] plays the determining role in the cleavage process.

Synergy on linear DNA formation mediated by the meta-*dicopper structure*: Besides the enhanced nicking efficiency, complex **1**, with the *meta*-dicopper motif, showed the ability to mediate formation of linear DNA in the range of 2–20 μM [Cu^{2+}] (Figure 4a, lanes 4–7), while complexes **2** and **4**, without the *meta*-dicopper motif, could not induce any linear DNA. On the other hand, complex **3**, possessing a lower nicking efficiency, can also mediate formation of linear DNA in the range of 12–45 μM [Cu^{2+}]. Its efficiency to induce formation of linear DNA was also decreased with the presence of the third copper center, since a higher [Cu^{2+}] was required to generate similar linear DNA than for complex **1**. On the other hand, it made complex **3** a more controllable reagent to generate linear DNA. It seems that the *meta*-dicopper motif is the essential structural factor to mediate formation of linear DNA.

The formation of linear DNA requires two cleavage sites on opposing strands within 10 bp of each other,[6d] and can be accomplished through either a double-stranded break or two independent single-stranded breaks of the opposing strands of supercoiled DNA.[24] The coexistence of all three forms of DNA in gel obtained in time-course experiments (Table 5) implied that the linear DNA induced by complexes **1** and **3** was formed mainly through double-stranded breaks (Figure S7 in the Supporting Information).[25–27] A standard statistical analysis by using the Poisson distribution and Freifelder–Trumbo relation found that the ratio of $n1/n2$ (where $n1$, $n2$, are the number of single-stranded breaks and double-stranded breaks per DNA molecule) ranged from 15.1 (3 min) to 18.3 (5 min) in the cleavage mediated by 8 μM of complex **3**.[7,25,28] For complex **1** (2 μM), the ratio of $n1/n2$ was 38.9 (5 min). It has been proposed that if the ratio of $n1/n2 > 100$, then the cleavage is purely random for pUC19 plasmid DNA.[7] The ratios of $n1/n2$ in our case were significantly less than 100, suggesting the formation of linear DNA mediated by complexes **1** and **3** should undergo a mainly non-random cleavage path.

The DNA cleavage modes promoted by external reagents are mainly affected by their DNA binding modes and the microstructure around the binding sites.[2,29] The binding modes not only alter the secondary structure of DNA but also affect the ROS to access the target proton of deoxyribose. Comparison of the different DNA cleavage behaviors promoted by these copper complexes suggests the double-stranded DNA lesion by complexes **1** and **3** may be related to their *meta*-dicopper motifs that form a *cleft* structure and affect their DNA binding mode. It is reported that the neocarzinostatin (NCS) molecule binds to the minor groove in a suitable mode, causing the two radicals of the same NCS molecule to react synergistically with the two adjacent deoxyribose units from the complementary strands of DNA and thus leads to the double-stranded lesion.[29] A similar event may also occur in the cases of complexes **1** and **3**, the DNA-bound ROS formed by complexes **1** and **3** may also react simultaneously with two complementary strands. However, various copper complexes with different structures have been found to mediate double-stranded cleavage,[6d,7,16,26] it is still unknown why the *meta*-dicopper motif favors this kind of cleavage. Further experimental and theoretical study on the DNA binding mode may help to clarify the present results.

Conclusion

The DNA cleavage behavior of water-soluble complexes **1–3** implied the synergy between metal centers on DNA cleavage could be dependent on the geometry of the metal centers. The synergy between copper centers in *meta*-dicopper or *para*-dicopper motifs leads to higher activity to generate nicked DNA from supercoiled pUC19 DNA. The third copper center in complex **3** leads to the decrease of DNA cleavage activity, although it has the highest DNA binding affinity amongst the three. Different from complex **2**, both complexes **1** and **3** mediated the formation of linear DNA, suggesting the *meta*-dicopper motif is required for such a cleavage. The geometrical dependence in DNA cleavage could be related to two events: DNA binding and O_2 activation. Although further study is necessary to clarify the present results, the current data demonstrate that the geometrical optimization of the polynuclear copper centers may lead to artificial nucleases with high and selective DNA cleavage. Moreover, the fact that *meta*-dicopper motif favors the generation of linear DNA through double-stranded cleavage may make such a structural motif applicable in the design of anticancer drugs that are usually double-stranded DNA cleavage promoters.[30]

Experimental Section

Materials and characterizations: Reagents such as methanol, chloroform, anhydrous Et_2O, $CuCl_2{\cdot}2H_2O$ were of analytical grade and were used without further purification. The 2,2′-dipicolylamine, *m*-xylylenedibromide, and 1,3,5-tris(bromomethyl)benzene were prepared according to the reported procedures,[31,32] The pUC19 plasmid DNA was purchased from TaKaRa Biotechnology (Dalian). The disodium salt of calf thymus DNA (CT DNA), tris(hydroxymethyl)aminomethane (Tris), and ethidium bromide (EB) were purchased from Sigma. The electrospray mass spectra were recorded using an LCQ electrospray mass spectrometer (ESMS, Finnigan) and Isopro 3.0 was used to simulate the isotopic distribution patterns of the assigned ions. Electrochemical measurements were performed at 25 °C on a EG&G PAR Model 273 potentiostat by using a standard three-electrode system comprising of a glass–carbon working electrode, a platinum-wire auxiliary electrode, and a Ag/AgCl reference electrode with 0.1 M aqueous KCl solution as the supporting electrolyte. The infrared spectra were recorded on a Bruker VECTOR22 spectrometer as KBr pellets (4000–500 cm^{-1}), and elemental analysis was performed on a Perkin–Elmer 240 C analytical instrument.

Synthesis of complexes

*m*TPXA and *p*TPXA were prepared by a literature method.[33] The ligand *N*,*N*,*N*′,*N*′,*N*″,*N*″-hexakis(2-pyridyl)-1,3,5-tris(aminomethyl)benzene) (HPTAB) was prepared by following a similar procedure used by Anslyn and co-workers with chloroform as the solvent instead of acetonitrile.[14] The eluent for gel chromatography was $CHCl_3/CH_3OH$ (30:1 *v*/*v*). ^{1}H NMR (500 MHz, $CDCl_3$, 25 °C, TMS): $\delta = 8.50$ (d, $J = 4.55$ Hz, 6H; Py-H_6), 7.57–7.61 (m, 12H; Py-H_3, -H_4), 7.38 (s, 3H; Bz-H), 7.11 (t, $J =$ 5.2 Hz, 6H; Py-H_5), 3.82 (s, 12H; NCH_2Py), 3.70 ppm (s, 6H; NCH_2Bz).

[Cu_2(*m*TPXA)Cl_4]·3H_2O (1): A mixture of $CuCl_2$·2H_2O (0.137 g, 0.8 mmol) and *m*TPXA (0.2 g, 0.4 mmol) in methanol (10 mL) was stirred for 1 h at room temperature and then was concentrated to 1 mL. Et_2O (8 mL) was added to the concentrated solution and the precipitate was collected by filtration and washed with acetone and Et_2O (0.296 g, 90%). IR (KBr pellet): $\tilde{\nu} = 1610$ cm^{-1} (C–N); MS (ES, positive): *m*/*z*: 349.2 $[M-2Cl]^{2+}$, 732.9 $[M-Cl]^+$ (M = Cu_2(*m*TPXA)Cl_4); elemental analysis calcd (%) for $C_{32}H_{38}Cl_4Cu_2N_6O_3$ (823.6): C 46.63, H 4.61, N 10.20; found: C 46.68, H 4.63, N 10.24.

[Cu_2(*p*TPXA)Cl_4]·3H_2O (2): Compound **2** was synthesized by a similar procedure as that for [Cu_2(TPmx)Cl_4]. Yield: 85%. IR (KBr pellet): $\tilde{\nu} =$ 1609 cm^{-1} (C–N); MS (ES, positive): *m*/*z*: 349.2 $[M-2Cl]^{2+}$, 732.9 $[M-Cl]^+$ (M = Cu_2(*p*TPXA)Cl_4); elemental analysis calcd (%) for $C_{32}H_{38}Cl_4Cu_2N_6O_3$ (823.6): C 46.63, H 4.61, N 10.20; found: C 46.72, H 4.60, N 10.18.

[Cu_3(HPTAB)Cl_5]·3H_2O·Cl (3): A mixture of $CuCl_2$·2H_2O (0.205 g, 1.2 mmol) and HTPAB (0.284 g, 0.4 mmol) in methanol (10 mL) was stirred for 2 h at room temperature. Then the solids were collected by filtration. After washing with acetone and diethyl ether, the dried solids were redissolved in aqueous acetonitrile (10% volume), and blue crystals suitable for X-ray structural determination were obtained by diffusion of acetone into the solution. Yield: 0.421 g, 90%. IR (KBr pellet): $\tilde{\nu} =$ 1607 cm^{-1} (C–N); MS (ES, positive): *m*/*z*: 336.3 $[M-3Cl]^{3+}$, 521.9 $[M-2Cl]^{2+}$, 1078.8 $[M-Cl]^+$ (M = Cu_3HPTABCl_6); elemental analysis calcd (%) for $C_{45}H_{51}Cl_6Cu_3N_9O_3$ (1169.4): C 46.18, H 4.36, N 10.77; found: C 46.28, H 4.38, N 10.82.

[Cu(BPA)Cl_2]·2H_2O (4): A mixture of $CuCl_2$·2H_2O (0.43 g, 2.51 mmol) and BPA (0.5 g, 2.51 mmol) in methanol (15 mL) was stirred for 1 h at room temperature, then the solids were filtered and washed with acetone and diethyl ether, and dried in air. Green crystals of complex **4** were obtained by vapor diffusion of diethyl ether into a solution of the complex in methanol. Yield: 0.696 g, 75%. IR (KBr pellet): $\tilde{\nu} = 3070$ (N–H), 1607 cm^{-1} (C–N); MS (ES, positive): *m*/*z*: 297.2 $[M-Cl]^+$, 630.7 $[2M-Cl]^+$ (M = Cu(BPA)Cl_2); elemental analysis calcd (%) for $C_{12}H_{17}Cl_2CuN_3O_2$ (369.8): C 38.94, H 4.60, N 11.36; found: C 38.85, H 4.62, N 11.39.

X-ray crystallography

For complexes **2** and **3**, a single crystal of the complex was mounted on a glass fiber. Intensity data were collected at 293 K on a Bruker SMART CCD area detector diffractometer operating in the ϕ-ω scan mode with graphite-monochromated $Mo_{K\alpha}$ radiation ($\lambda = 0.71073$ Å). Empirical absorption corrections were carried out by using a multiscan program.[34] The structures were solved by direct methods and refined on F^2 by full-matrix least-squares methods by using the SHELXTL program.[35] All the non-hydrogen atoms were located and added anisotropically. Hydrogen atoms were located and added to the structure. The data collection and refinement parameters of the two are given in Tables 1 and 2.

CCDC-281 821–281 822 contain the supplementary crystallographic data for this paper. These data can be obtained free of charge from the Cambridge Crystallographic Data Center via www.ccdc.cam.ac.uk/data_request/cif.

Spectroscopic studies on CT DNA binding ability

The binding of complexes to CT DNA has been studied by the fluorescent spectral method through the detection of the emission intensity of ethidium bromide (EB) on an AMINCO Bowman Series 2 luminescence spectrometer. The stock solution of calf thymus (CT) DNA (stored at 4 °C and used for not more than 4 d) was prepared in 5 mM Tris-HCl/50 mM NaCl in water, pH 7.4, and the concentration of the CT DNA was determined according to its absorption intensity at 260 nm with a known molar extinction coefficient value of 6600 M^{-1} cm^{-1}, and the ratio of UV absorbance at 260 and 280 nm, A_{260}/A_{280}, was 1.8–1.9, indicating that the DNA was sufficiently free of protein.[36] The experiments were done by adding 0~70 μM complexes into the EB-bound DNA or pure EB solution in Tris-HCl/NaCl buffer (pH 7.4), and the fluorescence was measured and normalized to 100% relative fluorescence.

Circular dichroism spectroscopic studies were performed by using a Jasco J-810 automatic recording spectropolarimeter. All determinations were made with a continuous flow of nitrogen purging the polarimeter, and the measurements were performed at room temperature with 1 cm pathway cells. The CD spectra were run from 320–220 nm at a speed of 10 nm min^{-1} and the buffer background was automatically subtracted. Data were recorded at an interval of 0.1 nm. The CD spectrum of DNA alone (100 μM) was recorded as the control experiment together with the CD spectra of DNA in the presence of complex at various ratios.

DNA cleavage experiments

The cleavage of DNA was studied by agarose gel electrophoresis. Supercoiled pUC19 DNA (200 ng) in Tris-HCl buffer (50 mM) containing 50 mM NaCl (pH 7.4) was treated with copper complexes and 1 μL of 3-mercaptopropionic acid (MPA) at a 100-fold molar excess relative to the complex to yield a total volume of 10 μL.[13] The mixtures were then incubated for 30 min at 37 °C. The reaction was quenched by the addition of 1 μL loading buffer, and then the resulting solutions were loaded on a 0.7% agarose gel. Electrophoresis was carried out at 50 mV for 2 h in TAE buffer (40 mM Tris acetate/1 mM EDTA). Bands were visualized under UV light and photographed. The quantification of each form of DNA was made by densitometric analysis of ethidium bromide containing agarose gel. A correction factor of 1.47 was used for supercoiled DNA (form I) taking into account the weak intercalation of EB to SC compared to nicked (form II) and linear DNA (form III).[7]

The cleavage of pUC19 plasmid DNA in the presence of standard radical scavengers and reaction inhibitors has also been studied. In these experiments, DMSO (as a hydroxyl radical scavenger), or 10 mM NaN_3 (as a singlet oxygen scavenger), or 10 mM KI (as hydrogen peroxide scavenger) was added to the solution of supercoiled DNA and the copper complexes. The mixture was incubated at 37 °C for 15 min prior to the addition of MPA to initiate the reaction, then the subsequent treatment and analysis followed the procedure described above.

Acknowledgements

We thank the National Natural Science Foundation of China (Grants 20231010, 20228102, 30370351, 20571043) and the Nature Science Foundation of Jiangsu province (BK2005209) for financial support.

[1] a) M. M. Meijler, O. Zelenko, D. S. Sigman, *J. Am. Chem. Soc.* **1997**, *119*, 1135–1136; b) E. L. Hegg, J. N. Burstyn, *Coord. Chem. Rev.* **1998**, *173*, 133–165; c) K. E. Erkkila, D. T. Odom, J. K. Barton, *Chem. Rev.* **1999**, *99*, 2777–2796; d) J. A. Cowan. *Curr. Opin. Chem. Biol.* **2001**, *5*, 634–642; e) C. Liu, M. Wang, T. Zhang, H. Sun, *Coord. Chem. Rev.* **2004**, *248*, 147–168; f) F. Mancin, P. Scrimin, P. Tecilla, U. Tonellato, *Chem. Commun.* **2005**, 2540–2548.

[2] *Chem. Rev.* **1998**, *98*, 937–1262: thematic issue (no. 3) on RNA/DNA cleavage.

[3] G. Pratviel, J. Bernadou, B. Meunier, *Adv. Inorg. Chem.* **1998**, *45*, 251–311.

[4] D. R. Graham, L. E. Marshall, K. A. Reich, D. S. Sigman, *J. Am. Chem. Soc.* **1980**, *102*, 5419–5421.

[5] S. Goldstein, G. Czapski, *J. Am. Chem. Soc.* **1986**, *108*, 2244–2250.

[6] a) S. T. Frey, H. H. J. Sun, N. N. Murphy, K. D. Karlin, *Inorg. Chim. Acta* **1996**, *242*, 329–338; b) K. J. Humphreys, K. D. Karlin, S. E. Rokita, *J. Am. Chem. Soc.* **2001**, *123*, 5588–5589; c) K. J. Humphreys, K. D. Karlin, S. E. Rokita, *J. Am. Chem. Soc.* **2002**, *124*, 6009–6019; d) K. J. Humphreys, A. E. Johnson, K. D. Karlin, S. E.

Rokita, *J. Biol. Inorg. Chem.* **2002**, *7*, 835–842; e) K. J. Humphreys, K. D. Karlin, S. E. Rokita, *J. Am. Chem. Soc.* **2002**, *124*, 8055–8066; f) K. D. Karlin, N. Wei, B. Jung, S. Kaderli, P. Niklaus, A. D. Zuberbühler, *J. Am. Chem. Soc.* **1993**, *115*, 9506–9514.

[7] Y. Jin, J. A. Cowan, *J. Am. Chem. Soc.* **2005**, *127*, 8408–8415.

[8] a) M. P. Suh, M. Y. Han, J. H. Lee, K. S. Min, C. Hyeon, *J. Am. Chem. Soc.* **1998**, *120*, 3819–3820; b) C. E. Yoo, P. S. Chae, J. E. Kim, E. J. Jeong, J. Suh, *J. Am. Chem. Soc.* **2003**, *125*, 14580–14589; c) A. Bencini, E. Berni, A. Bianchi, C. Giorgi, B. Valtancoli, D. K. Chand, H.-J. Schneider, *Dalton Trans.* **2003**, 793–800.

[9] Y. Gultneh, A. R. Khan, D. Blaise, S. Chaudhry, B. Ahvazi, B. B. Marvey, R. J. Butcher, *J. Inorg. Biochem.* **1999**, *75*, 7–18.

[10] M. Yashiro, A. Ishikubo, M. Komiyama, *Chem. Commun.* **1997**, 83–84.

[11] M. J. Young, D. Wahnson, R. C. Hynes, J. Chin, *J. Am. Chem. Soc.* **1995**, *117*, 9441–9447.

[12] S. Kawahara, T. Uchimaru, *Eur. J. Inorg. Chem.* **2001**, *7*, 2437–2442.

[13] M. Yashiro, H. Kaneiwa, K. Onaka, M. Komiyama, *Dalton Trans.* **2004**, 605–610.

[14] M. Komiyama, S. Kina, K. Matsumura, J. Sumaoka, S. Tobey, V. M. Lynch, E. Anslyn, *J. Am. Chem. Soc.* **2002**, *124*, 13731–13736.

[15] S. I. Kirin, C. M. Happel, S. Hrubanova, T. Weyhermüller, C. Klein, N. Metzler-Nolte, *Dalton Trans.* **2004**, 1201–1207.

[16] C. Tu, Y. Shao, N. Gan, Q. Xu, Z. J. Guo, *Inorg. Chem.* **2004**, *43*, 4761–4766.

[17] A. W. Addison, T. N. Rao, J. Reedijk, J. Rijn, C. C. van Verschoor, *J. Chem. Soc. Dalton Trans.* **1984**, 1349–1356.

[18] M. Lee, A. L. Rhodes, M. D. Wyatt, S. Forrow, J. A. Hartley, *Biochemistry* **1993**, *32*, 4237–4245.

[19] K. Karidi, A. Garoufis, N. Hadjiliadis, J. Reedijk, *Dalton Trans.* **2005**, 728–734.

[20] D. S. Sigman, *Biochemistry* **1990**, *29*, 9097–9105.

[21] a) K. D. Karlin, P. L. Dahlstrom, S. N. Cozzette, P. M. Scensny, J. Zubieta, *J. Chem. Soc. Chem. Commun.* **1981**, 881–882; b) M. S. Nasir, K. D. Karlin, D. McGowty, J. Zubieta, *J. Am. Chem. Soc.* **1991**, *113*, 698–700; c) N. N. Murthy, M. Mahroof-Tahir, K. D. Karlin, *J. Am. Chem. Soc.* **1993**, *115*, 10404–10405; d) K. D. Karlin, P. Ghosh, R. W. Cruse, A. Farooq, Y. Gultneh, R. R. Jacobson, N. J. Blackburn, R. W. Strange, J. Zubieta, *J. Am. Chem. Soc.* **1988**, *110*, 6769–6780.

[22] a) J. E. Bulkowski, P. L. Burk, M. F. Ludmann, J. A. Osborn, *J. Chem. Soc. Chem. Commun.* **1977**, 498–499; b) P. L. Burk, J. A. Osborn, M.-T. Youinou, Y. Angus, R. Louis, R. Weiss, *J. Am. Chem. Soc.* **1981**, *103*, 1273–1274.

[23] M. Suzuki, H. Furutachi, H. Okawa, *Coord. Chem. Rev.* **2001**, *200–202*, 105–129.

[24] C. Sissi, F. Mancin, M. Gatos, M. Palumbo, P. Tecilla, U. Tonellato, *Inorg. Chem.* **2005**, *44*, 2310–2317.

[25] L. F. Povirk, W. Wubker, W. Kohnlein, F. Hutchinson, *Nucleic Acids Res.* **1977**, *4*, 3573–3579.

[26] M. S. Melvin, J. T. Tomlinson, G. R. Saluta, G. L. Kucers, N. Lindquist, R. A. Manderville, *J. Am. Chem. Soc.* **2000**, *122*, 6333–6334.

[27] J. Drak, N. Iwasawa, S. Danishefsky, D. M. Crothers, *Proc. Natl. Acad. Sci. USA* **1991**, *88*, 7464–7468.

[28] D. Freifelder, *Biopolymers* **1969**, *7*, 681–693.

[29] I. H. Goldberg, *Acc. Chem. Res.* **1991**, *24*, 191–198.

[30] L. F. Povirk, *Mutat. Res.* **1991**, *257*, 127–143.

[31] a) G. S. Matouzenko, A. Bousseksou, S. Lecocq, P. J. van Koningsbruggen, M. Perrin, O. Kahn, A. Collet, *Inorg. Chem.* **1997**, *36*, 2975–2981; b) W. Wilhelm, *J. Org. Chem.* **1952**, *17*, 523–528.

[32] J. Y. Li, D. Liu, Y. Q. Li, C. S. Lee, H. L. Kwong, S. Lee, *Chem. Mater.* **2005**, *17*, 1208–1212.

[33] S. Kawahara, T. Uchimaru, *Eur. J. Inorg. Chem.* **2001**, 2437–2442.

[34] G. M. Sheldrick, SADABS, version 2, Multi-Scan Absorption Correction Program, Universität Göttingen, Göttingen (Germany), **2001**.

[35] G. M. Sheldrick, SHELX-97, A Computer Program for Crystal Structure Solution and Refinement, Universität Göttingen, Göttingen (Germany), **1997**.

[36] J. Marmur, *J. Mol. Biol.* **1961**, *3*, 208–214.

Received: January 12, 2006
Published online: June 6, 2006

